Materials Research. 2024; 27:e20240079
DOI: https://doi.org/10.1590/1980-5373-MR-2024-0079

Fly ash applied as Combined Extender Pigment and Carrier of Inhibitor-loaded LDH

***Janine R. Viscardi*[a], *Edilson V. Benvenutti*[b], *Lucas Bonan Gomes*[c],**

***Gerhard H. Knörnschild*[a,*], *Luís F. P. Dick*[a]**

[a]*Universidade Federal do Rio Grande do Sul, Escola de Engenharia, Laboratório de Processos Eletroquímicos e Corrosão, Av. Bento Gonçalves, 9500, 91501970, Porto Alegre, RS, Brasil.*
[b]*Universidade Federal do Rio Grande do Sul, Instituto de Química, Laboratório de Sólidos e Superfícies, Av. Bento Gonçalves, 9500, 91501970, Porto Alegre, RS, Brasil.*
[c]*Universidade Federal do Rio Grande do Sul, Inst. Geociências, Laboratório de Difratometria de Raios X, Av. Bento Gonçalves, 9500, 91501970, Porto Alegre, RS, Brasil.*

Received: February 16, 2024; Revised: June 04, 2024; Accepted: June 08, 2024

Fly ash (FA) was used successfully as a carrier for the corrosion inhibitor molybdate and applied as an extender pigment in an epoxy coating. To enhance interaction, molybdate was attached to FA through intercalation in layered double hydroxide (LDH), facilitated by surface modification of FA. Molybdate was incorporated into LDH either via direct synthesis or ion exchange. Directly synthesized LDH significantly increased molybdate storage in FA. The FA-inhibitor combination was tested in three ways: molybdate release kinetics, corrosion of an ultra-low carbono (ULC) steel in chloride solution, protection of ULC steel conferred by particles embedded in an epoxy coating. Short-term molybdate release was favored by ion exchange, long-term release by deglomeration of LDH. ULC steel corrosion inhibition in 0.1 M NaCl reached 89%. Incorporating the material into epoxy coatings mitigated steel corrosion, validated by electrochemical impedance spectroscopy. This study underscores the efficacy of FA-LDH-molybdate systems in corrosion protection.

Keywords: *Fly ash, LDH, molybdate, inhibitor carrier, coating, corrosion.*

1. Introduction

Fly ash (FA) is a byproduct of coal combustion in power plants and consists of spherical hollow particles with diameters ranging from 0.5 to 300 µm. The particles are captured in electrostatic precipitators and fabric filter bags to prevent their release into the atmosphere. Despite the concern about the impact of CO_2 emissions on global warming, energy production based on coal burning is still growing in some big economies, principally in China and India[1]. Therefore, enormous quantities of coal combustion products, like FA, will still emerge for many years and must be disposed of or reused. Today, reutilization as an additive for energy-intensive cement production is the leading destination of FA[2], apart from the disposal as landfill or structural fill supporting buildings or bridges. FA is also a cheap feedstock for products like fire bricks, cermet composites, thermal isolating layers, and catalytic action polymers.

FA consists of spherical particles in the micrometer range, which makes them a promising additive for protective coatings like paints. FA spheres are mostly hollow and can lower the total weight of a coating when applied to large surface areas such as those from airplanes and ships: The paint applied to (only parts of) the surface of a Boeing 747 weighs more than 250 kg, in the case of big ships the paint sums up many tons[3]. The density of hollow FA spheres is up to three times lower than that of dry paint[4-6]. Consequently, substituting 30% of the paint volume with hollow FA spheres might lead to a weight reduction of up to 20%.

Although little research has been made about FA as an additive in paints, some advantages of its use have been previously reported: Barpanda et al.[7] pointed out improved wear resistance of epoxy resin when FA was added. Song et al.[8] whitened FA by eliminating iron oxides and unburnt carbon to replace white TiO_2 pigment in paints. Dahalan et al.[9] substituted up to 40% of zinc pigment in an epoxy coating by FA as a low-cost extender pigment, still showing that the epoxy coating has good corrosion resistance. This example shows, however, that applying a reasonably high quantity of FA in paints means at least the partial substitution of some other pigments, which might have a function for corrosion protection. Therefore, the combination of FA with a corrosion inhibitor seems indicated.

In the present work, FA was combined with inhibitor-bearing layered double hydroxides (LDH).

These layered materials can be described as anionic clays, whose structure is similar to the mineral hydrotalcite ($Mg_6Al_2(OH)_{16}CO_3 \cdot 4H_2O$). Brucite-like octahedral sheets where M^{3+} substitutes M^{2+} cations possess an excess positive charge, compensated by anions, such as the inhibitor molybdate, intercalated in the galleries between the sheets[10,11].

Various researchers have already shown the feasibility of using LDH as a carrier for corrosion inhibitors[12-18]. When FA spheres serve as a host for inhibitor-bearing LDHs, the interaction FA-LDH can happen in different ways:

*e-mail: gerhard.hans@ufrgs.br

- LDHs can be deposited at the outer surface of the spheres.
- if a chemical or mechanical impact opens hollow spheres, LDH deposition might be extended to the inner surface.

FA comprises varying portions of SiO_2, Al_2O_3, Fe_2O_3, CaO, and unburnt carbon. Combinations of octahedral sheets with tetrahedral silicate ones are frequently observed in natural clay minerals[19]. Therefore, the interaction of LDH with Si-rich FA spheres can be expected.

In this work, we studied the fabrication of inhibitor carriers for application in paints starting from FA spherules. Molybdate was then directly deposited on FA as well as intermediated by LDH. The release of the inhibitor and its efficiency were determined as a function of the inhibitor carrier preparation method. The feasibility of combining inhibitor-loaded FA with epoxy paint was evaluated by electrochemical impedance measurements (EIS).

2. Materials and Methods

2.1. Sampling and FA preparation

Eletrobras-CGT Eletrosul, Candiota, Brazil, provided the FA directly collected from the electrostatic precipitator.

A sample of FA was previously sieved in the fractions: coarser than # 170, coarser than #325, between # 325 and # 400, and finer than # 400. The fraction between # 325 and # 400 was washed with distilled water and subjected to an ultrasound bath of distilled water for 30 min.

2.2. Surface modification of FA by chemical treatment

FA was subjected to chemical treatments in HNO_3, HF, and NaOH to increase the surface area, chemically modify the surface, and eventually open the FA spheres by localized chemical attack.

FA was stirred for 12 h in different nitric acid concentrations (0.1, 0.5, 1.0, 5.0 M) at a 10 g/100 mL FA to solution ratio to increase the surface area, remove magnetite, and possibly open the plerospheres. Afterward, the FA was washed with deionized water to pH ≈ 7, filtered, and dried at 100 °C.

FA was attacked with 0.5 and 5.0 M HF solutions at a 10 g /100 mL FA to solution ratio. The mixture with 0.5 M HF solution was stirred for 1 h. After that, the material was washed 5 times with 50 mL of filtered distilled water, followed by ultrasonic cleaning in 100 mL of ethanol. The attacked material was filtered and dried at 100 °C for 1 h. The attack with 5.0 M HF was carried out under mechanical stirring for 16 h, followed by the same procedures used in the other acid attacks.

FA was also subjected to an alkaline attack with 0.1 M and 5.0 M NaOH solutions at a 10 g/100 mL FA/solution ratio sonicated for 5 min. Then, the FA was washed with deionized water to pH ≈ 7, filtered, and dried at 100 °C.

2.3. Application at FA of the inhibitor molybdate

Molybdate was applied to the pigment FA by the following four methods:

- Direct exposure of molybdate to FA: Mo@FA;
- LDH growth at the FA surface followed by MoO_4^{2-} incorporation by ion exchange into LDH under aerobic conditions: Mo-LDH@FA(non-inert)
- LDH growth at the FA surface followed by MoO_4^{2-} incorporation by ion exchange into LDH in N_2-atmosphere: Mo-LDH@FA(inert), and
- direct synthesis of LDH by precipitation in a molybdate-containing solution, Mo-LDH@FA(dir-synt.).

This preparation methods are described below.

2.3.1. Mo@FA

2 g of FA, previously treated with 5 M HNO_3 solution, was weighed, and 40 mL of 0.1 M sodium molybdate dihydrate ($Na_2MoO_4.H_2O$) solution was added. The mixture was kept under stirring for 96 h. After this period, the material was filtered and oven-dried at 100 °C for 2 h.

2.3.2 Mo-LDH@FA(non-inert)

Briefly, Mg-Al LDH was grown on the FA substrate with a Mg^{2+}/Al^{3+} molar ratio of 2:1. For the precipitation of LDH, 5.14 g of FA were added to 100 mL of a 0.05 M $Mg(NO_3)_2 6H_2O$ + 0.025 M $Al(NO_3)_3 \cdot 9H_2O$ solution. 150 ml of a 0.1 M $NaNO_3$ solution were added dropwise to this mixture. The pH of the obtained slurry was held at 10 during the synthesis by adding 1 M NaOH solution. The reaction was conducted at 65 °C for 24 h under constant stirring. The precipitate was washed to pH 7, filtered, and dried at 100 °C. For the intercalation of the corrosion inhibitor into the LDH structure, an anion exchange reaction was performed in a glass reactor using 4 g of FA with deposited LDH by stirring in 40 mL of 0.1 M $Na_2MoO_4.H_2O$ solution for 24 h at room temperature. After that, the LDH with the inhibitor species was filtered and dried at 100 °C. The synthesis was conducted in a non-inert atmosphere (open reaction cells exposed to atmospheric CO_2).

2.3.3. Mo-LDH@FA(inert)

In this case, the above-described sample preparation was conducted under N_2 purging, avoiding exposure to carbonate from the atmosphere.

2.3.4. Mo-LDH@FA(dir-synt.)

A so-called direct synthesis was also performed by adding 5.142 g of FA to 100 ml of a 0.25 M $Na_2MoO_4.H_2O$ solution and then slowly adding 100 mL of 0.05 M $Mg(NO_3)_2 \cdot 6H_2O$ + 0.025 M $Al(NO_3)_3 \cdot 9H_2O$ in a reactor. The pH was adjusted to 10 with a 1 M NaOH solution and allowed to react for 24 h at 65 °C under stirring and N_2 purging. The precipitate was finally filtered and dried at 100 ° C. Dissolved CO_2 and Carbonate formation from atmospheric CO_2 and its intercalation into LDH lamellae were minimized by boiling the deionized water before solution preparation.

For the sake of comparison, samples of molybdate-loaded LDH were also produced by the same direct synthesis process, however, in the absence of FA.

2.4. Characterization

The size distribution of FA particles was determined using low-angle laser light scattering with a *CILAS 1190*

device. Particle morphology was imaged using *JEOL JSM 6060* and *Zeiss EVO MA10* scanning electron microscopes (SEM). For this, FA and LDH samples were suspended in 1 mL of ethanol and deposited on a polished stub previously metalized with gold. Microanalysis (EDS) was performed on the same equipment, but in this case, graphite stubs were used to lower the substrate influence.

X-ray diffraction (XRD) patterns were acquired from powder samples using a *Siemens /Bruker AXS-D-5000* diffractometer with Cu K_α radiation. The X-ray patterns were analyzed using the Rietveld refinement and *Maud* software. Around 12 wt% LiF was added as a standard to the FA samples, and its percentage was proportionally subtracted from the final result.

The specific surface area and the microporous size distributions of FA were estimated at various processing stages using the Brunauer, Emmett e Teller (BET), and Density Functional Theory (DFT) methods. For the analyses, the *Micromeritics Tristar II Kr 3020* equipment was used. The nitrogen adsorption and desorption isotherms were obtained at the nitrogen boiling temperature. For this, samples were previously heated to 120 °C under vacuum for 12 h.

2.5. Preparation of epoxy resin

The epoxy used for coating preparation was a bi-component epoxy system without any pigments (clear coating). Component A used was *Araldite® GZ 7071 X 75*, and component B was *450BD.* Two sets of clear coating were prepared: the blank system and Mo-LDH@FA (dir-synt.) doped with 10 wt% particles.

The epoxy coating was applied to ULC steel samples using the immersion technique. The coated samples were exposed to the atmospheric conditions for 7 days to cure the epoxy coating. The thicknesses were quantified using a dry film thickness gauge with a fixed sensor, BYK Gardner, model Byko-test 7500. The final thickness of the dry films was 100 - 130 μm for all samples. Circular defects with a diameter of about 630 μm were made by drilling to study the release of corrosion inhibitor from the coating.

2.6. Inhibitor release tests

FA and synthesized species were analyzed by Inductively Coupled Plasma Optical Emission Spectroscopy (ICP-OES) to determine their molybdate content based on the US EPA 3052 method[20]; however, a digester block was used in the procedure. For digestion, 100 mg of solid sample were put in a PTFE tube containing 1 mL of conc. HF + 1.5 mL conc. HCl + 0.5 mL conc. HNO_3 and heated to 60 °C for 30 min. Finally, the mixture was heated to 120 °C to dry and evaporate residual HNO_3 and HF. Finally, 20 mg of H_3BO_3 and 1.5 mL conc. HCl + 0.5 mL conc. HNO_3 was added to remove eventual fluoride rests and complete the digestion, respectively, and the solution was heated to 120 °C for 2 h in a closed PTFE tube.

The molybdate release was tested at room temperature by adding 1 g of the prepared sample to 99 mL of a pH 6.8 buffer solution (20 mM NaH_2PO_4 + 2.91 mM NaOH) containing 0.1 M NaCl). Release tests were also performed in a pH 4.6 buffer (20 mM NaH_2PO_4 + 0.1 M NaCl) and the same pH 4.6 buffer without chloride addition. 0.5 mL aliquots were sampled with a micropipette for up to 81 days of immersion or until stabilization of the released molybdate. Then, the solution was filtered through polycarbonate membranes and analyzed using inductively coupled plasma optical emission spectrometry (ICP-OES of *Agilent Technologies, model 5110*). The release tests of samples prepared by direct synthesis were also performed in the same solutions, using molybdate-loaded LDH prepared by the same method, however without FA. For the sake of comparison, the mass of these samples was modified to have the same available quantity of molybdate as in the respective release tests with FA.

2.6. Corrosion tests

The corrosion tests were performed with ULC (C < 0.005%) steel. Samples with a geometric area of approximately 0.8 cm^2 were cut and polished to # 1200, washed with distilled water and ethanol, dried, and then stored under a vacuum. Cyclic voltammetry (CV) was performed in a three-electrode electrochemical cell with a Pt grid as the counter electrode and an Ag/AgCl in 1 M NaCl reference electrode. However, all potentials are referred to the Standard Hydrogen Electrode (SHE). CV tests were performed with and without Mo-LDH@FA(dir-synt.) containing 0.1 M NaCl. The specimen was immersed after 24 h of inhibitor release, and CV was started after 3 h of immersion when the open circuit potential had stabilized.

EIS measurements were performed in a three-electrode cell where Ag/AgCl/0.1 M NaCl was used as the reference electrode, a platinum counter electrode, and the coated samples as working electrodes with an exposed área of 4.9 cm^2 and a circular defect area of $2.8x10^{-3}$ cm^2. The electrolyte was a 10 mL drop of 0.1 M NaCl deposited on the coating defect at room temperature. The frequency ranged from 3 mHz to 100 kHz. The amplitude of the applied signal was 10mV.

3. Results and Discussion

3.1. FA characterization

Figure 1 shows FA's typical particle size distribution in the "as received" condition determined by laser diffraction: The particle size ranges from 0.29 to 580 μm, with a significant fraction in the 28—112 μm interval. 10% of the particles are smaller than 6.7 μm, 50% than 45.0 μm, and 90% than 161.6 μm. The average diameter of FA particles is 72.9 μm.

The mean particle composition determined by EDS for the as-received FA was ($_{at}$%): 3.4 C, 68.0 O, 0.3 Na, 0.4 Mg, 7.2 Al, 19.0 Si, 0.01 S, 0.8 K, 0.4 Ca, 0.03 Ti, 0.5 Fe. Most of the particles are cenospheres of different sizes, as the SEM images of Figure 2a show. Plerospheres (spheres packed with other spheres) and irregular porous carbonaceous particles are also present. Carbonaceous particles result from incomplete oxidation of the precursor coal, according to Diamond[21].

The residual carbon of FA samples was removed by flouting in deionized water, while the magnetite/hematite fraction was by simple magnetic separation followed by an acid attack with 5.0 M HNO_3. Thus, the surface area determined by BET expresses rather the properties of the FA. Figure 2b shows the fraction of FA particles after sieving between 325 and 400 mesh (44-36 μm), the desired size

range for the pigments used (indicated in Figure 1**).** After the acid treatment, most of the particles remained intact, as observed by SEM; others had slight recesses, and some had holes on the surface (Figure 2c).

XRD of each FA size fraction allowed the identification of the crystalline phases after sieving. Table 1 quantifies the phases obtained by the Rietveld refinement using internal standards. Quartz, mullite, hematite, and calcite were identified (Table 1)[22]. The amorphous phases have higher content in the coarser particle fraction. The amorphous species might be attributed to silica particles formed by quenching a high-viscosity melt[23], possibly containing elements other than Si, such as K and Na, as indicated by the EDS analysis. Hematite and calcite of this particle size fraction were eliminated by the acid attack with 5 M HNO_3 solution (Table 1), which also caused a substantial decrease in the mullite content. Decomposition and dissolution of these phases led, on the other hand, to a substantial increase of the amorphous silica, while the quartz content diminished relatively.

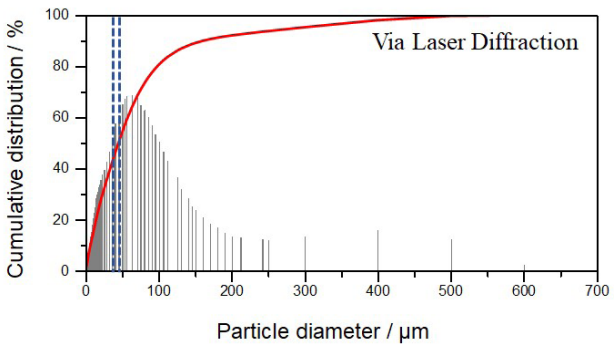

Figure 1. FA particle size distribution in the as-received condition obtained by laser diffraction. Die blue dotted lines indicate the used size range.

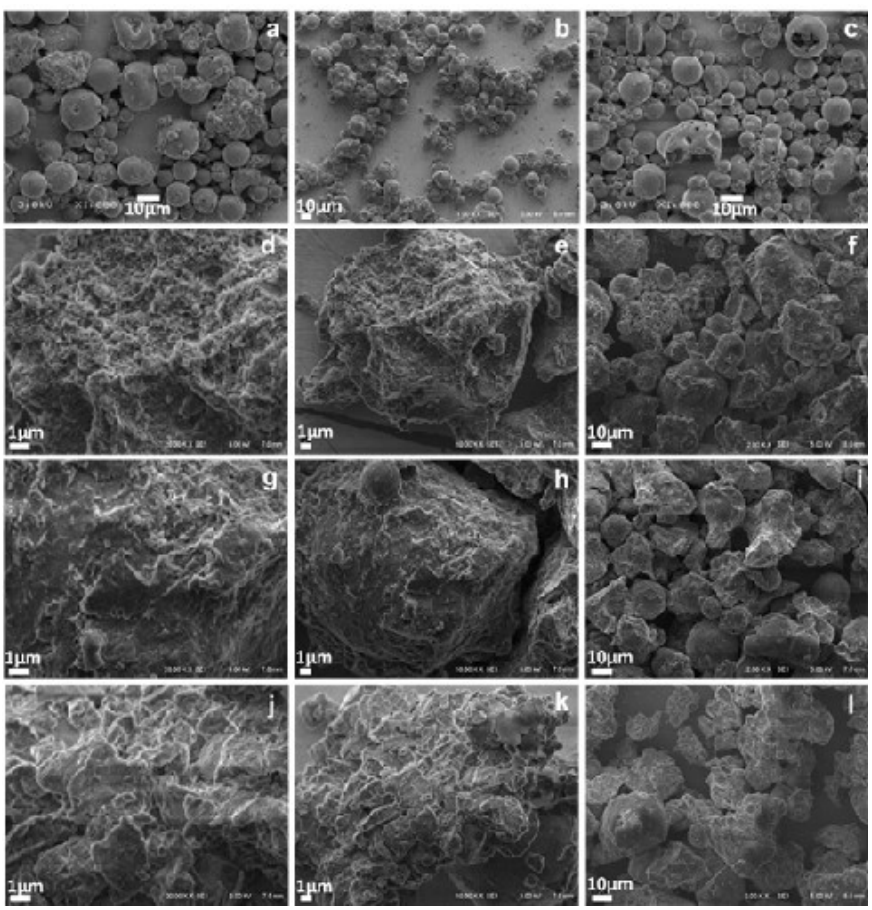

Figure 2. SEM micrographs of FA with and without deposited LDH. FA: (a) as-received; (b) sieved between 325 and #400; (c) after 12 h in 5 M HNO3, 24 ˚C, and sieved between 325 and #400. FA with deposited LDH: (d-f) Mo-LDH@FA(non-inert); (g-i) Mo-LDH@FA(inert); (j-l) Mo-LDH@FA(dir-synt).

Table 1. Percentage of phases determined by the Rietveld refinement for each size fraction of the FA before and after the acid attack (12 h, 5 M HNO_3, 25 °C), sieve classified before XRD).

Phase	>#170	>#325	#325-400	<#400	#325-400 attacked
	(wt.%)	(wt.%)	(wt.%)	(wt.%)	(wt.%)
Quartz	16.9	20.7	24.5	19.3	17.9
Mullite	14.8	31.6	31.3	39.2	7.8
Hematite	-	16.1	0.9	0.6	-
Calcite	9.3	1.3	5.5	7.2	-
Amorphous	59.0	30.3	37.8	33.7	74.3

3.2. Synthesis, characterization, and inhibitor intercalation of LDH

The structure of LDH synthesized by the three sample preparations, Mo-LDH@FA(non-inert), Mo-LDH@FA(inert), and Mo-LDH@FA(dir-synt), was verified by XRD (Figure 3). Quartz and mullite from the FA substrate remain visible in the diffractograms after LDH deposition. The diffractograms of (a) Mo-LDH@FA(non-inert), (b) Mo-LDH@FA(inert), (c) Mo-LDH@FA(dir-synt) and (d) Mo-LDH(dir-synt.) demonstrate the typical pattern of hydrotalcite-like minerals, whose structure typically consists of layers of mixed Me (II) – Me (III) hydroxides, separated by that of anions and water molecules.

In the diffractogram of the synthesis performed under non-inert condition, Figure 3a, the peaks were more intense than that performed under N_2 purge, Figure 3b, indicating that a lower amount of LDH was deposited under this condition.

For the synthesis in a non-inert atmosphere, the basal plane interplanar spacing d_{003} calculated with the corresponding diffraction peak at 11.5° is 7.7 Å, close to 7.6 Å, the value reported in the literature when $(CO_3)^{2-}$ is intercalated[10]. The carbonate anion stabilizes the brucite-like sheets, hindering ion exchange. The conditions under which LDH synthesis is carried out are decisive for the results obtained. The measured d_{003} value of 8.6 Å for LDH grown in the inert atmosphere indicates that nitrate anions are intercalated during its synthesis[10].

Various authors report d_{003} interplanar spacings resulting from the intercalation of different anions between the hexagonal basal planes (001)[12,15,24-30]. However, the species released by LDH can either be the ion incorporated into the crystalline structure or adsorbed at the outer side of the LDH lamellae[15], enhanced by the high specific area of the nano lamella. Compared with literature data[12,15,24-30], the d_{003} values measured in the present study after ion exchange indicate that there was no complete insertion of the inhibitor between the basal planes or there was only adhesion of species on the surface of the structure. For the direct synthesis, however, the interplanar spacing of 9.6 Å points to the presence of intercalated molybdate ions (Figure 3c**)**. Molybdate ions were also intercalated when the same direct synthesis was performed in the absence of FA since the same interplanar spacing was found in this case (Table 2).

The crystallite size of the deposited LDH lamellae can be determined using the expression derived by Scherrer (Equation 1):

$$L_{hkl} = \frac{K\lambda}{\beta cos\theta} \quad (1)$$

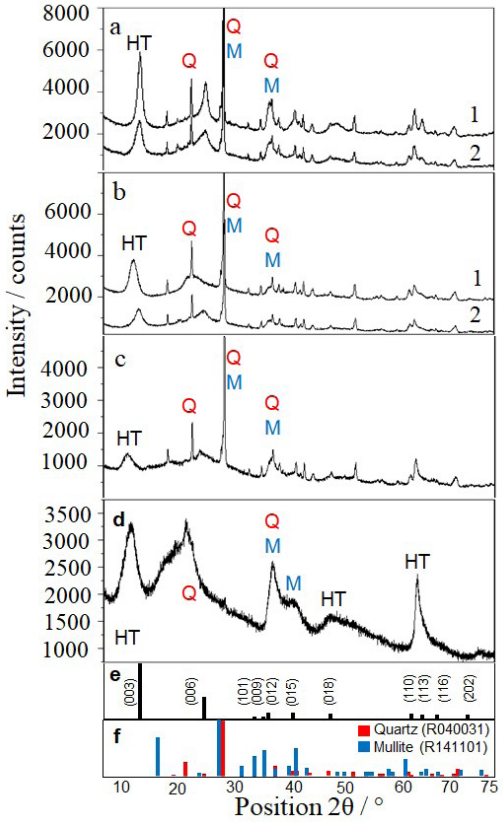

Figure 3. XRD spectra: (a) Mo-LDH@FA(non-inert); (1) before ion exchange, (2) after ion exchange, (b) Mo-LDH@FA(inert); (1) before ion exchange, (2) after ion exchange, (c) Mo-LDH@FA(dir-synt), (d) Mo-LDH(dirsynt), (e) hydrotalcite, and (f) Mullite (blue lines) and quartz (red lines) standards according to RRUFF [21].

Where L_{hkl} is the mean crystallographic size in the specific *hkl* direction, K, the shape factor, λ, the wavelength of the X-ray beam (Cu k λ , 1.54178 Å), and β the full width at half maximum (FWHM) of this *hkl* peak. Equation 1 was applied to the orthogonal directions <003> and <110> before and after the molybdate anion intercalation procedure using the FWHM values obtained from reflections 003 and 110. Additional peaks were used to check the values obtained from low-index peaks when possible.

Initially, a general value of 0.91 was suggested for the shape factor K. More recently, Lim et al.[31] showed that the estimated error for the hexagonal habit of carbon flakes using the same basal plane peaks is lower than ± 5% when

using K' = 2 in the modified Scherrer equation proposed by Lim et al.[31] (Equation 2) for dimensions greater than about 10 nm. The constant c in this equation can be chosen according to the shape, usually taken as c = 1.6 nm. The so-calculated crystallite sizes (Table 2) depend on the nucleation and growth kinetics of the LDH layers on the FA substrate. The spectral width was determined using a LaB_6 standard for crystallite size calculations. The value for each angular range was subtracted from the FWHM of reflections 003 and 110.

$$L_{hkl} = K' \frac{\lambda}{\beta cos\theta} - c \quad (2)$$

The crystallite size of LDH grown in the absence of FA, Mo-LDH(dir.synt.), was noticeably smaller than that in the presence of FA (Table 2). It can be assumed that FA favors instantaneous nucleation of LDH, leading to larger LDH crystallites on its surface, while in the absence of FA, nucleation is slow and continuous. Then, crystallites of varying sizes lead to broader peaks in the X-ray spectrum without FA (Figure 3d).

The formation of the LDH layer on the FA can be seen in Figure 2d-l. The FA particles were previously mostly spherical and smooth. With the growth of the LDH layer, the surface became irregular and rough. Due to the small dimension of the LDH crystallites, isolated particles cannot be resolved in the SEM. The total change of the surface morphology indicates that deposition of LDH has occurred at nearly the entire surface with the agglomeration of LDH crystallites.

3.3. LDH Texture analysis of the FA-LDH composites

The textural analysis of FA samples was performed using N_2 adsorption-desorption isotherms shown in Figure 4a, c to study the effect of chemical attack with NaOH, HNO_3, and HF, respectively, of various concentrations. The FA in the as-received condition presents a BET surface area of 0.7 $m^2 g^{-1}$, similar to values reported by Külaots et al.[32] for nine coal FA types obtained from various US facilities. The attack of FA with 5M NaOH increased the surface area to 1.5 $m^2 g^{-1}$, while the one with 5M HF led to 6.0 $m^2 g^{-1}$, and that with 5M HNO_3 to 2.7 $m^2 g^{-1}$, respectively.

Moreover, DFT pore distribution curves show for 5M HNO_3 (Figure 4b) the presence of nanopores[33] with a diameter lower than 20 Å, while for 5M HF, micro and mesopores can be identified (Figure 4d). The chemical attack in 5M HNO_3 also leads to the partial opening of FA spheres. However, the surface area increase is much higher than that which might be caused by sphere opening (at most two times). Therefore, the increase in surface area must be mainly attributed to the formation of micropores.

Although the high surface area might be advantageous for posterior LDH deposition, the toxicity of HF[34] and its corrosive nature make it less suitable for applications in corrosion inhibition. Moreover, siliceous residues precipitated during the HF treatment caused an undesired agglomeration of the FA spheres. On the other hand, an attack by 5 M HNO_3 produced a higher concentration of amorphous silica (see Table 1), which might be favorable for the interaction with LDH. Therefore, HNO_3 was chosen as the preferred treatment.

The N_2 adsorption-desorption isotherms for the samples with LDH are depicted in Figure 4e. The desorption brand of the isotherms presents H3 hysteresis, typical of the presence of slit pores[26]. This hysteresis occurs when the evaporation is delayed until reaching the critical pressure ($P/P_0 \sim 0.45$) and the meniscus collapses, producing total desorption of the gas and, consequently, the closure of the hysteresis loop[35]. In the present case, the slit pores represent the vacant space between the agglomerated lamellar LDH crystallites.

3.4. Elemental analysis of FA before and after molybdate deposition

EDS analysis was performed on the surface of the FA attacked by 5 M HNO_3 before and after molybdate deposition using the methods described above (Table 3). Attacked FA shows a high Si content due to mullite, quartz, amorphous phase, and Al from mullite. At the same time, the Mg concentration is below 1 at.%, and Mo was not detected. After the deposition of molybdate carrying LDH, the Mg concentration increased to more than 11 at.%, demonstrating the LDH presence, while the Al concentration did not change noticeably compared to the FA surface. However, Al now comes from LDH rather than from the FA substrate. In all analyses of samples with deposited LDH, a Mo concentration between 1 and 3 at.% was detected. Generally, the concentration found in Mo-LDH@FA(dir-synt.) was slightly higher than Mo in the other two preparations with LDH. When molybdate was directly deposited on the FA, the Mo concentration was so low that it could not be detected in the spectrum. The EDS spectrum shows essentially the composition of the FA substrate in this case.

Table 2. Interplanar spacings d_{003} and d_{110}, FWHM values, and crystallite sizes (L_{hkl}) calculated using modified Scherrer equation[24] and mean aspect ratio a.r. (L_{110}/L_{003}).

Sample	d_{003}	FWHM	L_{003}	d_{110}	FWHM	L_{110}	a.r
	/Å	/ °	/nm	/Å	/°	/nm	.
LDH @FA (non-inert)	7.7	0.9	17.7	1.5	0.5	43.5	2.5
Mo-LDH@FA (non-inert)	7.6	0.9	17.9	1.5	0.4	46.2	2.6
LDH@FA (inert)	8.6	1.5	10.5	1.5	0.4	46.8	4.5
Mo-LDH@FA (inert)	7.9	1.6	9.8	1.5	0.5	40.1	4.1
Mo-LDH@FA (dir-synt)	9.6	1.8	8.6	1.5	0.5	37.8	4.4
Mo-LDH (dir-synt)	9.6	1.6	6.4	1.5	1.3	13.1	2.0

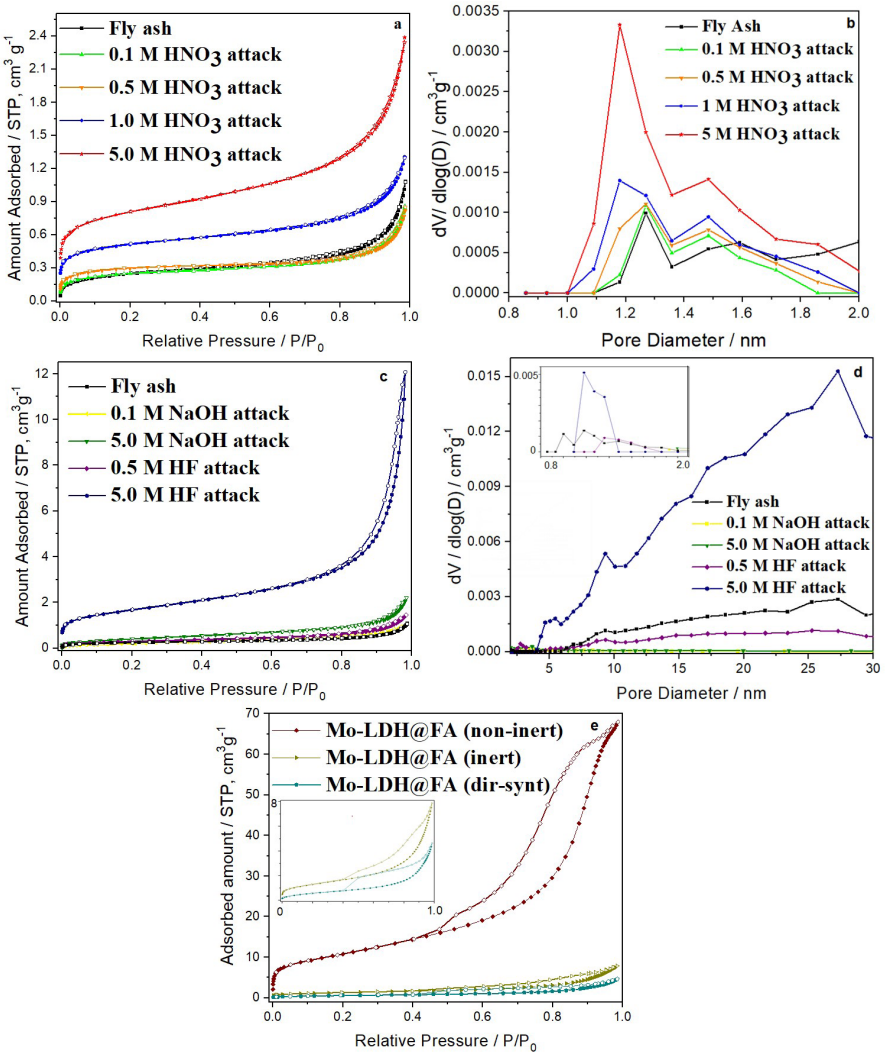

Figure 4. N2 adsorption-desorption isotherms of FA: a) HNO3 treated samples; b) DFT micropore size distribution curves of fly ash treated with HNO3 solutions; c) N2 adsorption-desorption isotherms of textural analysis of NaOH and HF treated FA samples; d) DFT pore size distribution curves of NaOH and HF treated FA samples. The inset in Figure 4d highlights the micropores region. e) N2 adsorption-desorption isotherms of LDH deposited on FA treated with 5 M HNO3.

Table 3. EDS analysis of FA before and after deposition of molybdate (elements with less than 1 at.% in FA were omitted).

Element (at.%)	FA	Mo@FA	Mo-LDH@FA (non inert)	Mo-LDH@FA (inert)	Mo-LDH@FA (dir-synt)
O	70.4	71.4	77.0	81.4	73.6
Na	0.3	0.2	-	-	1.6
Mg	0.4	0.4	13.6	11.3	13.0
Al	7.5	6.1	6.2	4.6	6.9
Si	20.0	19.5	2.2	0.5	2.2
Mo	-	-	1.0	2.2	3.0

3.5. Microscopic analysis after ion milling

LDH crystallites synthesized in the presence of FA are deposited in significant quantities on the surface of FA spheres, as Figure 2 shows. Most of the original FA surface is covered due to the agglomeration of LDH particles.

In order to verify the LDH deposition inside hollow FA spheres, Mo-LDH@FA(dir-synt.) specimens were submitted to Ar+ ion milling (15 min, 5 ° incidence angle, 5 µA, 3 keV). Arbitrarily chosen FA spheres, opened by sputtering, were examined microscopically (Figure 5**)**. Various EDS analyses of deposited material inside the FA spheres detected Mo, Mg, and Al, thus attesting the presence of LDH carrying molybdate also inside FA (Figure 5a-c). Analysis Figure 5d represents the section of the FA wall where molybdate was not detected. The number of spheres with molybdate inside was higher than the few open spheres occasionally found in

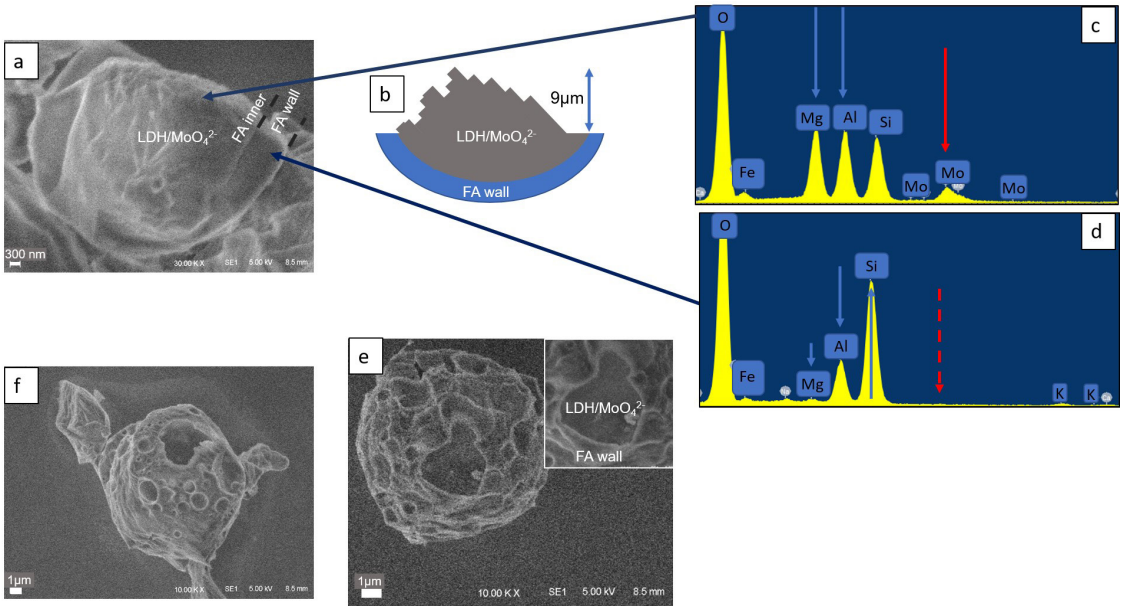

Figure 5. Damage induced in Mo-LDH@FA(dir-synt) by ion milling: a) LDH crystallites inside FA; b) height of the LDH layer within the FA measured by focal length; c) EDS inside the FA containing LDH lamellae; d) EDS on the external wall of FA; e) LDH precipitates inside FA particle; f) hollow interior of LDH@FA.

untreated FA. Thus, the treatment in 5 M HNO_3 led to the opening of some FA spheres by local chemical attack. However, from the examined number of spheres, it was impossible to quantify the part of FA spheres opened due to the chemical attack. The surface area of the FA spheres became about four times higher by the attack of HNO_3, according to the BET measurements. Since sphere opening can raise the surface area by two at most, the principal part of the increase is caused by surface roughening. More examples of opened FA spheres and precipitates inside are shown in Figure 5e, f.

3.6. Available molybdate for release

After molybdate incorporation, the inhibitor release in buffer solutions with and without NaCl was measured by ICP-OES. All tests were performed until the accumulated molybdate release was constant. Before the release tests, the presence of molybdate as an impurity of the original samples was quantified. The samples from the *Candiota Thermoelectric* in the as-received condition contained 0.66 mg MoO_4^{2-} (0.4 mg Mo)/g FA, decreasing to 0.03 mg MoO_4^{2-} (0.02 mg Mo)/g FA after the acid attack with 5 M HNO_3. Thus, Mo detected after FA functionalization can be attributed to inhibitor release.

As shown in Figure 6a-d, the MoO_4^{2} quantity available for release depends strongly on the sample preparation mode. When molybdate was directly deposited on the FA without LDH (Mo@FA), $1.41 \cdot 10^{-5}$ mol Mo/g was detected (Figure 6a). However, the quantity of molybdate in the samples prepared via LDH deposition was between one and two orders of magnitude higher: $8.78 \cdot 10^{-4}$ mol Mo/g by ion exchange in a non-inert atmosphere (Figure 6b), $4.88 \cdot 10^{-4}$ mol Mo/g in an inert atmosphere (Figure 6c), and $9.44 \cdot 10^{-4}$ mol Mo/g of sample prepared by direct LDH synthesis with molybdate (Figure 6d).

The direct interaction of molybdate with the FA surface is weak, leading to a low quantity of molybdate adsorbed on the FA surface. Molybdate can be intercalated in the interplanar galleries of LDH or attached to the external surface of the LDH crystallites. For Mo@FA(dir-synt.), the $d_{(003)}$ distance of 9.6 Å strongly indicates that molybdate is intercalated in the interplanar galleries of LDH. The intercalated molybdate might explain the highest value of available molybdate. On the other hand, in a non-inert atmosphere, ion exchange leads to nearly no modification of the d_{003}. The d_{003} distance of 7.6 Å for Mo@FA(non-inert) samples is compatible with intercalated carbonate ions, indicating that molybdate is essentially present at the external surface of LDH or inside agglomerated LDH/FA composites.

Nevertheless, the quantity of molybdate available in the Mo@FA(non-inert) samples is nearly as high as that in Mo-LDH@FA(dir-synt.) samples. The latter have intercalated molybdate but less molybdate at the external surface. An intermediate value of 7.9 Å was measured for the d_{003} distance of Mo-LDH@FA(inert), meaning the intercalation of molybdate was incomplete. Despite the inert atmosphere during preparation, some carbonate might have been intercalated, or part of the nitrate ions remained intercalated. From the d_{003} value, intercalated carbonate and nitrate can hardly be distinguished. The partial intercalation of molybdate explains why Mo-LDH@FA(inert) samples have less available molybdate than Mo-LDH@FA(dir-synt.) samples. A comparison of Mo-LDH@FA(dir-synt.) with LDH produced under the same conditions but in the absence of FA showed the following: The molybdate content is similar in both cases when it is related to the LDH weight: Mo-LDH@FA(dir-synt.): 15,9wt.% of LDH is molybdate, Mo-LDH(dir-synt.): 15,0wt.% of LDH is molybdate.

3.7. Molybdate release from LDH

It was recently shown[13,15] that the molybdate release from LDH is initially controlled by ion exchange or diffusion.

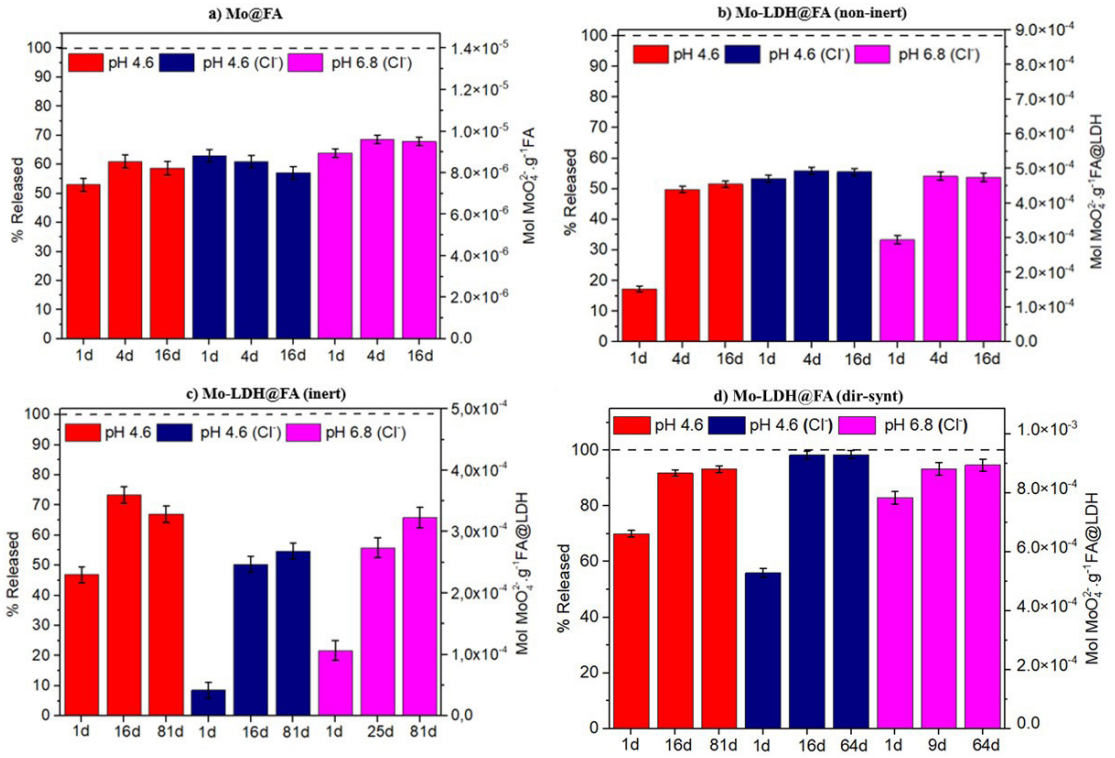

Figure 6. Molybdate released from 1 g of sample in the following electrolytes: phosphate buffer pH 6.8; phosphate buffer pH 4.6; phosphate buffer pH 4.6 + 0.1 M NaCl. First bar: release within 1 day; second bar: shows time to release quantity of molybdate equal to the total release; third bar: final time of measurement, showing that no further release has happened compared to the second bar, within the margin of error. The molybdate concentration at the right y-axis, equivalent to 100%, represents the total available molybdate.

What differentiates the present study from previous ones is that LDH loaded with inhibitor is agglomerated at the surface of the FA. A coagulating amorphous phase probably sticks together LDH crystallites carrying molybdate, as XRD indicated no additional crystalline phase. Therefore, molybdate from deeper zones within the agglomerate cannot be liberated directly to the electrolyte. It needs a deglomeration reaction consisting of slow chemical dissolution of the amorphous coagulant or the LDH itself. Fast release of molybdate, as reported previously, also happens here as a first step and is shown below for Mo-LDH@FA(dir-synt.) and Mo-LDH(dir-synt.). Molybdate from LDH at the surface of the agglomerate can be released directly to the bulk electrolyte. It might be deduced from the textural analysis that slit pores separate LDH crystallites. Molybdate can then be released to the bulk electrolyte by pore diffusion.

Release by these processes ceases essentially within less than 24 hours, as previous studies have shown[13,15]. However, in most of the cases studied in the present work, molybdate released after 24 h was well below the available quantity of inhibitor (Figsure 6a-d). Therefore, release tests were continued in order to monitor further releases. In the case of Mo@FA (Figure 6a), the quantity of molybdate released within 24 h is identical, within the error margin, with the total release measured during 16 days. Adsorbed molybdate is directly released from the FA surface; agglomeration does not occur. Even after 16 days, however, the released molybdate represents only 60% of the available quantity. Part of molybdate seems strongly bound to the FA surface, which hinders its release. Long-term release of molybdate due to slow deglomeration can be observed in the case of Mo-LDH@FA(inert) (Figure 6c), and Mo-LDH@FA(dir-synt.) (Figure 6d). Release of molybdate to the electrolyte ceased within 16 days, in one case within 25 days, as the second bar in each graph (Figure 6c, d) shows. Long-term release of inhibitor might be advantageous for a painted surface where the attack is by atmospheric corrosion and, consequently, the surface repeatedly comes in contact with small quantities of electrolyte rather than exposure to a bulk electrolyte.

Mo-LDH@FA(dir-synt.) released more than 90% of the available molybdate, showing that nearly complete deglomeration has occurred. From Mo-LDH@FA(inert), on the other hand, only 50-70% of the available molybdate was released. This might be caused by intercalated carbonate ions, which hinder the liberation of parts of the molybdate ions from the interplanar galleries. From Mo-LDH@FA(non-inert) samples, the liberation of molybdate ceased within four days (Figure 6b). At first sight, this seems to be caused by faster liberation of molybdate from the external surface of LDH when compared to intercalated molybdate liberation. However, if deglomeration is the necessary precondition for molybdate release, then the result shows a faster deglomeration reaction. Mo-LDH@FA(non-inert) was the only preparation mode executed in a CO_2-containing atmosphere. The hydrolysis of CO_2 contaminants resulted in the intercalation of carbonate

ions and might have also influenced the properties of the coagulant phase, leading to its faster decomposition. Once in contact with the electrolyte, the liberation of molybdate from the LDH is faster than the deglomeration reaction. Concerning deglomeration, no characteristic differences were observed between the electrolytes: phosphate buffer pH 6.8, phosphate buffer pH 4.6, and phosphate buffer pH 4.6 + 0.1 M NaCl. The time to complete the release is essentially independent of the electrolyte.

The release processes for the four sample preparations, described in the above paragraph are schematically explained in Figure 7.

Table 4 summarizes the data about molybdate release for the four preparation modes. It can be seen that Mo-LDH@FA(dir-synt.) is the most promising preparation, with the highest load of available inhibitor and the highest degree of total release. Mo-LDH@FA(dir-synt.) was therefore chosen for further studies about molybdate release and application in paint.

Release tests were completed for short times and the Mo-LDH@FA(dir-synt.) samples were compared to samples prepared by the same direct synthesis method, but in the absence of FA (Figure 8a). After one hour of release, 40-50% of the available molybdate was liberated in the chloride-containing buffer solutions, pH6.8 and pH4.6, versus 20-30% in the chloride-free buffer pH 6.8. The higher liberation in chloride-containing buffer continued during the following hours, but after eight hours, the differences had nearly ceased. The results might show that release during short times is controlled by ion exchange in the presence of chloride. Similar results in the presence of chloride were reported by Bendinelli et al.[15]. The comparison between LDH deposited on FA and LDH without FA does not show considerable differences concerning molybdate release in the two cases. As shown before, the presence of FA influences the LDH crystallite size. However, the crystallite size does not considerably influence the short-time release of molybdate, supporting the assumption that short-time release is controlled by ion exchange rather than diffusion.

Moreover, the comparison showed that the release of molybdate is not retarded when LDH is bound to the surface of FA. This is a promising result for the application in paints. Figure 8b shows the same comparison over extended time. It can be seen that, with and without FA, the total release of molybdate from samples prepared by direct synthesis is >90% of the available quantity. The diagram also reveals that in both cases, part of the molybdate is released by a slow process, meaning that agglomeration and deglomeration of LDH also happen in the absence of FA.

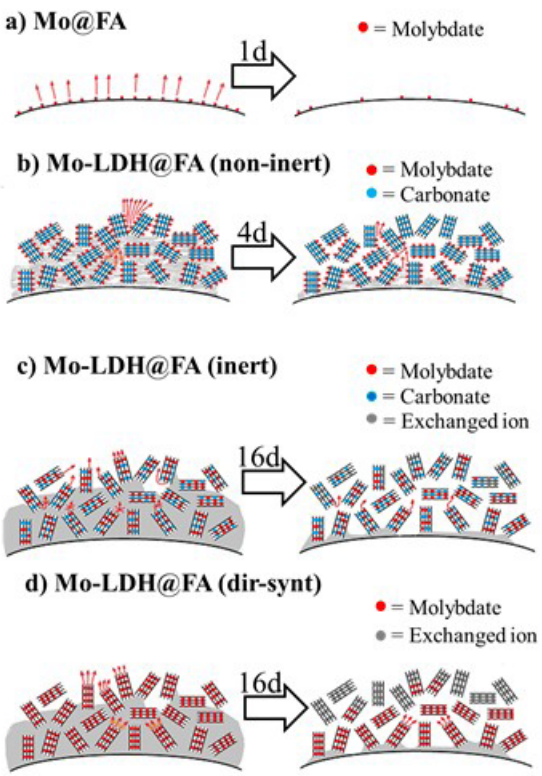

Figure 7. Schematic description of long-term release of molybdate as a function of preparation process.

3.8. Corrosion inhibition by molybdate liberated from LDH

The corrosion inhibition efficiency of molybdate carrying LDH@FA was tested on the bare surface of an ULC steel sheet in an air-saturated 0.1 M NaCl electrolyte. In the semilogarithmic diagram (Figure 9), the comparison of the steel in 0.1 M NaCl and 0.1 M NaCl with Mo-LDH@FA(dir-synt.) reveals a more substantial influence of the inhibitor on the anodic curve. The anodic partial currents in both electrolytes and at least the cathodic partial current in the electrolyte with MoLDH@FA(dir-synt.) show Tafel-like behavior. Thus, the cathodic reaction in the neutral electrolyte is charge transfer controlled oxygen reduction. These conditions allow the determination of corrosion currents by extrapolating the Tafel lines. In the electrolyte with Mo-LDH@FA(dir-synt.), an inhibitor efficiency (%IE) of 89% was observed, according to

$$IE = 100\% \frac{\left(i_{corr} - i_{corrinhib}\right)}{i_{corr}}$$

3.9. Corrosion behavior of epoxy coating containing functionalized FA

EIS measurements with samples of epoxy coating (pure, with FA, and with Mo-LDH@FA, all without circular artificial defect) of 100-130 µm thickness on ULC steel showed all

Table 4. Total available and released Molybdate/g (sample) and vs. sample preparation.

Preparation mode	Mo@FA	Mo-LDH@FA (non-inert)	Mo-LDH@FA (inert)	Mo-LDH@FA (dir-synt)
Available Molybdate/g(sample)	$1.41 \cdot 10^{-5}$ mol	$8.78 \cdot 10^{-4}$ mol	$4.88 \cdot 10^{-4}$ mol	$9.44 \cdot 10^{-4}$
Final release (%)	60-70	50-60	55-75	>90

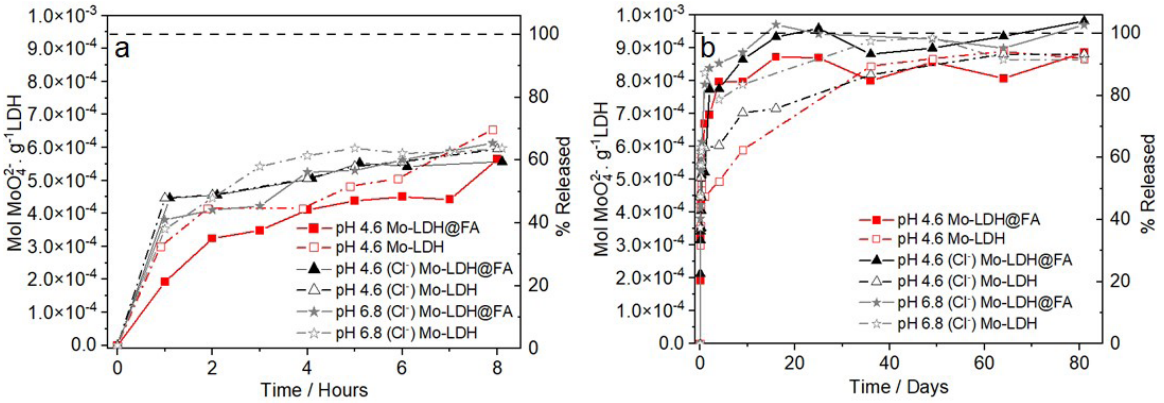

Figure 8. Molybdate released from samples prepared by direct synthesis. Comparison: LDH bound to FA (Mo-LDH@FA) vs. "free LDH" (Mo-LDH) a) Short-term release of molybdate b) Long-term release of molybdate.

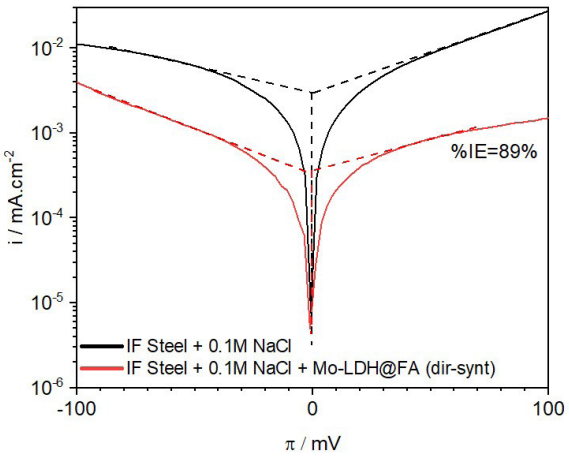

Figure 9. Polarization curves (i vs. π) of the IF steel after 3 hours without inhibitor (black lines) and Mo-LDH@FA(dir-synt) (red lines).

impedances >1 GΩcm^2 when measured in 0,1 M NaCl, 30 min after immersion. This means that FA and inhibitor-loaded LDH, when applied to the paint, did not cause macroscopic cracks or other structural defects during paint drying.

The steel samples coated with pure epoxy resin as well as epoxy with Mo-LDH@FA(dir-synt), both with a circular defect, were evaluated by EIS measurements during 24 h of immersion in 0.1 M NaCl solution, Figure 10. After 1 h of immersion the coating with Mo-LDH@FA(dir-synt.) with circular defect presented capacitive arcs of larger diameter in comparison with the pure resin. This indicates the release of inhibitor stored in the coating after the metal is directly exposed to the electrolyte at the mechanical defect. This behavior continues throughout the measurements. After 24 hours, the formation of a second capacitive arc can be observed in the Nyquist diagram, which may occur due to the formation of a protective film on the anodic sites due to the reaction of molybdate anions with oxidized metal cations[36]. In the Bode diagram |Z|, Phase vs. log(f), (Figure 10b, c), the emergence of a second process becomes visible already after 4 h, with an observed increase of |Z|, corroborating with a supposed protective film formation. Over the whole test time, the resin with Mo-LDH@FA(dir-synt.) has a higher |Z| than the pure resin, thus proving the efficiency of the developed material.

4. Conclusions

The present work showed the viability of a new corrosion protection system consisting of FA-supported LDH as a corrosion inhibitor carrier, where molybdate acted as the inhibitor. The studied process transforms a selected fraction of the industrial waste FA into a higher-value product, which can be added to paints. The stored quantity of molybdate can be increased up to two orders of magnitude when LDH is used as an intermediator for its storage. The inhibitor's stored quantity and release rate depend on details of how Mo-LDH@FA is assembled. Molybdate can be adsorbed at the outer surface of the LDH lamellae and intercalated in the interplanar galleries. The latter was observed when assembly occurred directly in a molybdate-containing solution (Mo-LDH@FA(dir-synt.)). This preparation method led to the highest amount of molybdate per sample weight available for release. LDH loaded with molybdate is agglomerated at the surface of FA spheres, externally and partially internally, in spheres opened by the chemical pretreatment in HNO_3.

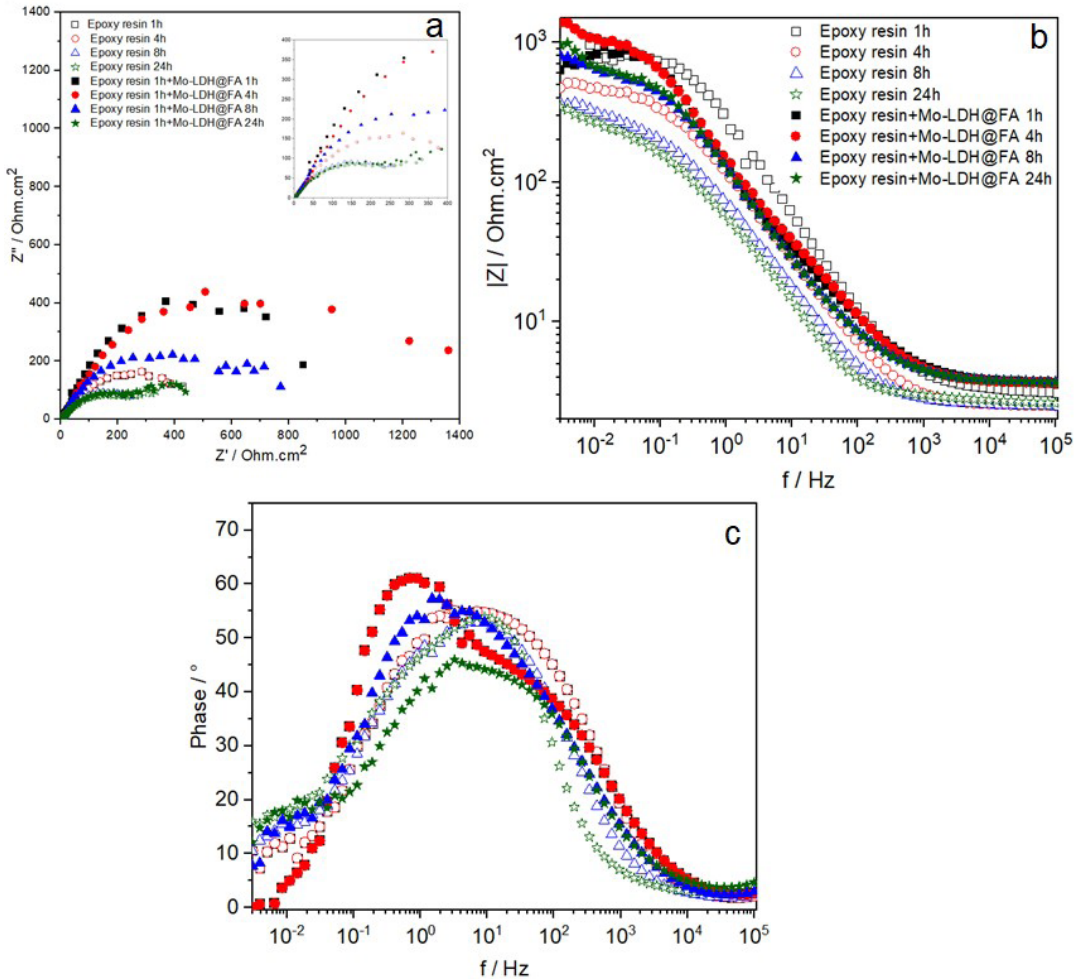

Figure 10. EIS diagrams a) Nyquist, b) Bode |Z| vs. f, c) Phase angle vs. f for interstitial free (IF) steel coated with an epoxy-based resin doped or not with 10wt.% (wet) of Mo-LDH@FA (dir. syn.) after a circular defect (2.8x10-3cm2) at different immersion times in 0.1 M NaCl.

When LDH enters into contact with the electrolyte, molybdate is released by fast processes involving ion exchange and diffusion[13,15]. Additionnally, the combination of LDH with FA leads to a slow release process, where the inhibitor is delivered for up to 25 days. The slow deglomeration reaction possibly controls this process. The efficiency as an inhibitor of molybdate liberated from LDH supported on FA was demonstrated by electrochemical tests in 0.1 M NaCl solution. EIS measurements corroborate the inhibitory effect caused by including Mo-LDH@FA(dir-synt.) in transparent epoxy resin after mechanical defects were introduced in the coating. Epoxy resin doped with Mo-LDH@FA showed capacitive arcs of larger diameter and greater resistance when compared to undoped material.

5. Acknowledgments

The authors greatly acknowledge Eletrobras CGT-Eletrosul. (Candiota, Brazil) for founding (CGTEE/SEDE/027/2018) and the Centro de Microscopia e Microanálise-UFRGS. J.R.V is grateful to CAPES/DS (Nº 88882.439205/2019-01- Finance code 001) for the fellowship.

6. References

1. Fastmarkets. Coaltrans Conference, global aspects on coal combustion products [Internet]. 2019 [cited 2021 May 19]. Available from: https://www.coaltrans.com/insights/article/global-aspects-on-coal-combustion-products
2. Lin B, Cerato AB, Madden AS, Madden MEE. Effect of fly ash on the behavior of expansive soils: microscopic analysis. Environ Eng Geosci. 2013;19:85-94.
3. Boeing. Painting versus polishing of airplane exterior surfaces [Internet]. 2023 [cited 2023 Nov 1]. Available from: www.boeing.com/commercial/aeromagazine/aero_05/textonly/fo01txt.html
4. Ranjbar N, Kuenzel C. Cenospheres: a review. Fuel. 2017;207:1-121.
5. Ghosal S, Self SA. Particle size-density relation and cenosphere content of coal fly ash. Fuel. 1995;74:522-9.
6. Shirai H, Ikeda M, Tanno K. Factors affecting the density and specific surface area (blaine value) of fly ash from pulverized coal combustion. Energy Fuels. 2011;25:5700-6.
7. Barpanda P, Kulkarni SM. Kishore. Sliding wear behaviour of an epoxy system reinforced with particulate fly ash filler. Adv Compos Lett. 2009;18:199-205.
8. Song H, Fan H, Gao H-T, Liu J-A, Mou H. Improving fly ash brightness with carbon and iron oxide removal. Recycling. 2020;5:5.

9. Dahalan ENE, Sofian AH, Abdullah A, Noor NM. Corrosion behavior of organic epoxy-xinc coating with fly ash as an extender pigment. Mater Today Proc. 2018;5:21629-35.
10. Cavani F, Trifirò F, Vaccari A. Hydrotalcite-type anionic clays: preparation, properties, and applications. Catal Today. 1991;11(2):173-301.
11. Ogino I, Hirayama Y, Mukai SR. Intercalation chemistry and thermal characteristics of layered double hydroxides possessing organic phosphonates and sulfonates. New J Chem. 2020;44:10002-10.
12. Nejati K, Akbari AR, Davari S, Asadpour-Zeynali K, Rezvani Z. Zn–Fe-layered double hydroxide intercalated with vanadate and molybdate anions for electrocatalytic water oxidation. New J Chem. 2018;42(4):2889-95.
13. Shkirskiy V, Keil P, Hintze-Bruening H, Leroux F, Vialat P, Lefèvre G, et al. Factors affecting MoO_4^{2-} inhibitor release from Zn_2Al based layered double hydroxide and their implication in protecting hot dip galvanized steel by means of organic coatings. ACS Appl Mater Interfaces. 2015;7(45):25180-92.
14. Montemor MF. Functional and smart coatings for corrosion protection: a review of recent advances. Surf Coat Tech. 2014;258:17-37.
15. Bendinelli EV, Rocha AC, Barcia OE, Aoki IV, Margarit-Mattos ICP. Effects of lamellar reconstruction routes in the release of molybdate encapsulated in Mg–Al layered double hydroxides. Mater Chem Phys. 2016;173:26-32.
16. Bendinelli E, Aoki IV, Barcia O, Margarit-Mattos ICP. Kinetic aspects of Mg-Al layered double hydroxides influencing smart corrosion protective behavior. Mater Chem Phys. 2019;238:121883.
17. Kuznetsov B, Serdechnova M, Tedim J, Starykevich M, Kallip S, Oliveira MP, et al. Sealing of tartaric sulfuric (TSA) anodized AA2024 with nanostructured LDH layers. RSC Advances. 2016;6:13942-52.
18. Salak NA, Tedim J, Kuznetsova AI, Zheludkevich ML, Ferreira MGS. Anion exchange in Zn-Al layered double hydroxides: in situ X-ray diffraction study. Chem Phys Lett. 2010;495:73-6.
19. Grim RE. Clay mineralogy. 2nd ed. New York: McGraw-Hill; 1968.
20. US EPA: U.S. Environmental Protection Agency. Method 3052: microwave assisted acid digestion of siliceous and organically based matrices [Internet]. Washington, D.C.: US EPA; 1996 [cited 2021 Oct 26]. Available from: https://www.epa.gov/sites/default/files/2015-12/documents/3052.pdf
21. Diamond S. Particle morphologies in fly ash. Cement Concr Res. 1986;16:569-79.
22. Lafuente B, Downs RT, Yang H, Stone N. The power of databases: the RRUFF project. In: Armbruster T, Danisi RM, editors. Highlights in mineralogical crystallography. Berlin: W. De Gruyter; 2015. p. 1-30. (Numbers: Quartz: R040031; Mullite: R141101; Hydrotalcite: R050457).
23. Kutchko B, Kim A. Fly ash characterization by SEM-EDS. Fuel. 2006;85:2537-44.
24. Ciocan CE, Dumitriu E, Cacciaguerra T, Fajula F, Hulea V. New approach for synthesis of Mo-containing LDH based catalysts. Catal Today. 2012;198:239-45.
25. Hulea V, Maciuca A-L, Fajula F, Dumitriu E. Catalytic oxidation of thiophenes and thioethers with hydrogen peroxide in the presence of W-containing layered double hydroxides. Appl Catal A Gen. 2006;313:200-7.
26. Guo L, Zhang F, Lu J-C, Zeng R-C, Li S-Q, Song L, et al. A comparison of corrosion inhibition of magnesium aluminum and zinc-aluminum vanadate intercalated layered double hydroxides on magnesium alloys. Front Mater Sci. 2018;12:198-206.
27. Zeng R-C, Liu Z-G, Zhang F, Li S-Q, Cui H-Z, Han E-H. Corrosion of molybdate intercalated hydrotalcite coating on AZ31 Mg alloy. J Mater Chem A Mater Energy Sustain. 2014;2:13049-57.
28. Zheludkevich ML, Poznyak SK, Rodrigues LM, Raps D, Hack T, Dick LF, et al. Active protection coatings with layered double hydroxide nanocontainers of corrosion inhibitor. Corros Sci. 2010;52:602-11.
29. Buchheit RG, Guan H, Mahajanam S, Wong F. Active corrosion protection and corrosion sensing in chromate-free organic coatings. Prog Org Coat. 2003;47:174-82.
30. Wang S, Liu C, Wang M, Chuang Y, Chiang P. Arsenate adsorption by Mg/Al–NO_3 layered double hydroxides with varying the Mg/Al ratio. Appl Clay Sci. 2009;43:79-85.
31. Lim DJ, Marks NA, Rowles MR. Universal Scherrer equation for graphene fragments. Carbon. 2020;162:475-80.
32. Külaots I, Hurt RH, Suuberg EM. Size distribution of unburned carbon in coal fly ash and its implications. Fuel. 2004;83:223-30.
33. Sing KSW, Everett DH, Haul RAW, Moscou L, Rouquerol J, Siemieniewska T. Reporting physisorption data for gas/solid systems with special reference to the determination of surface area and porosity. Pure Appl Chem. 1985;57:603-19.
34. Zhang Y, Wang X, Sharma K, Mao X, Qiu X, Ni L, et al. Injuries following a serious hydrofluoric acid leak: first aid and lessons. Burns. 2015;41:1593-8.
35. De Souza LV, Tkachenko O, Cardosoa BN, Pizzolato TM, Dias SLP, Vasconcellos MAZ, et al. Strategy to control the amount of titania dispersed on SBA-15 surface preserving its porosity, aiming to develop a sensor for electrochemical evaluation of antibiotics. Microporous Mesoporous Mater. 2019;287:203-10.
36. Bentley AJ, Earwaker LG, Farr JPG, Saremi M, Seeney AM. Molibdates in aqueous corrosion inhibitor – III. Effects of molybdate in the anodic filming of steel. Polyhedron. 1986;5(1-2):547-50.